IOP Publishing Plasma Sources Science and Technology
Plasma Sources Sci. Technol. **32** (2023) 115001 (17pp) https://doi.org/10.1088/1361-6595/ad0570

3D particle-in-cell simulations of negative and positive streamers in C_4F_7N–CO_2 mixtures

Baohong Guo[1], Ute Ebert[1,2] and Jannis Teunissen[1,*]

[1] Centrum Wiskunde & Informatica (CWI), Amsterdam, The Netherlands
[2] Department of Applied Physics, Eindhoven University of Technology, Eindhoven, The Netherlands

E-mail: jannis.teunissen@cwi.nl

Received 17 August 2023, revised 5 October 2023
Accepted for publication 20 October 2023
Published 2 November 2023

Abstract

We investigate negative and positive streamers in C_4F_7N–CO_2 mixtures through simulations. These mixtures are considered to be more environmentally friendly than the insulating gas SF_6 that is widely used in high voltage technology. Simulations are performed using a 3D particle-in-cell model. Negative streamers can propagate when the background field is close to the critical field. We relate this to their short conductive channels, due to rapid electron attachment, which limits their field enhancement. Positive streamers also require a background field close to the critical field, and in addition a source of free electrons ahead of them. In our simulations these electrons are provided through an artificial stochastic background ionization process as no efficient photoionization process is known for these gases. In 3D, we can only simulate the early inception stage of positive discharges, due to the extremely high electric fields and electron densities that occur. Qualitative 2D Cartesian simulations show that the growth of these discharges is highly irregular, resulting from incoming negative streamers that connect to existing channels. The inclusion of a stochastic background ionization process also has an interesting effect on negative discharges: new streamers can be generated behind previous ones, thereby forming a chain of negative streamers.

Keywords: streamer discharge, particle in cell, simulation, C_4F_7N mixture, insulation gas

1. Introduction

1.1. Eco-friendly alternative to the greenhouse gas SF_6

Sulfur hexafluoride (SF_6), an insulating gas, has been widely used in electric power equipment such as gas circuit breakers and gas-insulated switchgear [1], due to its excellent properties for electrical insulation and current interruption [2, 3]. But it is also the most potent industrial greenhouse gas, with a global warming potential (GWP) of about 23 500 times that of CO_2 over a 100 year horizon and an atmospheric lifetime of about 1000 years [4, 5]. Therefore there is an urgent need for exploring more sustainable alternatives. The most promising candidate is perfluoronitrile (C_4F_7N), an electronegative gas developed by the 3 M Company [6]. It has a relatively low GWP of about 1490, a relatively short atmospheric lifetime of about 22 years, good material compatibility with most electric power equipment, and a dielectric strength twice that of SF_6 [7]. Depending on the application, C_4F_7N is often mixed with buffer gases such as CO_2, N_2 or dry air, primarily due to its relatively high liquefaction temperature (e.g. $-4.7\,^{\circ}C$ at 0.1 MPa), considerations regarding environmental sustainability and safety, as well as cost reduction and availability [8].

1.2. Streamer discharges in C_4F_7N–CO_2 mixtures

Numerous theoretical and experimental investigations have been conducted to explore the electric breakdown and recovery properties of C_4F_7N mixtures for practical applications. The decomposition pathways of C_4F_7N have been

* Author to whom any correspondence should be addressed.

studied in [9–14]. Swarm parameters such as ionization and attachment coefficients have been experimentally measured to determine the reduced critical electric field and to estimate the dielectric strength of C_4F_7N mixtures [15–20]. Furthermore, their breakdown characteristics and dielectric properties have been extensively investigated through experimental measurements [21–30] as well as theoretical calculations [31–33]. C_4F_7N–CO_2 mixtures with approximately 10%–20% C_4F_7N have been found to achieve a comparable dielectric strength to SF_6 under varying conditions.

However, there are very few experimental studies on streamer discharges in C_4F_7N–CO_2 mixtures. This is primarily due to the challenge of imaging such discharges, given the lack of detectable light emission. Understanding streamer discharges in these mixtures is important, as they play a key role in the initial stage of electric breakdown [34]. Several authors have therefore computationally studied streamers in C_4F_7N–CO_2 mixtures with 2D fluid simulations [35–40], which will be further elaborated in section 5. The goal of this paper is to computationally study both negative and positive streamers in C_4F_7N–CO_2 mixtures in a full 3D geometry. In contrast to previous simulations in these mixtures, we use a 3D particle model which can capture the stochastic nature and branching of streamers in a more realistic way.

1.3. Cross sections for C_4F_7N

A set of electron–neutral collision cross sections is required as the model input for accurate modeling of streamers in C_4F_7N–CO_2 mixtures [41]. In recent years, numerous studies have been dedicated to obtaining cross section data for C_4F_7N through both theoretical and experimental methods [42].

The total electron impact ionization cross section of C_4F_7N was calculated using the Deutsch–Märk (DM) formalism [43] and the binary-encounter-Bethe (BEB) method [44]. To improve the agreement between these two methods, Zhong *et al* proposed to combine the DM and BEB formalisms with a dual sigmoid function [45]. In [46], the total and partial ionization cross sections of C_4F_7N were theoretically and experimentally studied. Furthermore, Chachereau *et al* estimated the total electron attachment cross section of C_4F_7N by inversely calculating swarm parameters obtained from a pulsed Townsend experiment [16]. The dissociative electron attachment process was also experimentally examined in [47], but no cross section data were given. In [48], Sinha *et al* utilized the spherical complex optical potential (SCOP) formalism to compute the total inelastic cross section of C_4F_7N, from which the electronic excitation and ionization cross sections were derived. The SCOP method was further used to calculate the elastic cross section of C_4F_7N in [49]. Note that the above-mentioned cross sections were all considered individually.

A complete set of electron–neutral collision cross sections for C_4F_7N has recently been proposed for the first time in [50], see figure 1, which will be used in the present paper. Beyond electron–neutral collisions, the ion kinetics including detachment and ion conversion may also influence the dielectric properties of C_4F_7N–CO_2 mixtures, but there is currently only limited data available on these processes [51].

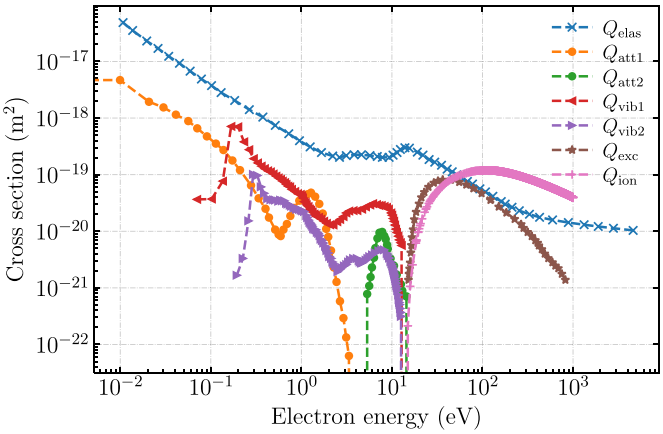

Figure 1. A complete set of electron–neutral collision cross sections for C_4F_7N from [50]. This set includes elastic cross section (Q_{elas}), electron attachment cross sections (Q_{att1}, Q_{att2}), vibrational excitation cross sections (Q_{vib1}, Q_{vib2}), electronic excitation cross section (Q_{exc}) and electron impact ionization cross section (Q_{ion}).

2. Simulation method

We simulate negative and positive streamers in C_4F_7N–CO_2 mixtures at 300 K and 1 bar. Simulations are performed with a 2D/3D PIC-MCC (particle-in-cell, Monte Carlo collision) model, using the open-source `Afivo-pic` code [52]. Below we give a brief summary of the model, see more information in [52, 53].

2.1. PIC-MCC model

2.1.1. Particle mover and collisions. Electrons are tracked as particles. Ions are included as densities and assumed to be immobile on the considered short time scales (up to 50 ns). Neutral gas molecules are present as a homogeneous background that electrons stochastically collide with.

In the electrostatic approximation, the positions $\mathbf{x}$ and velocities $\mathbf{v}$ of simulation particles are advanced in time with the 'Velocity Verlet' scheme [54] as

$$\boldsymbol{x}(t+\Delta t) = \boldsymbol{x}(t) + \Delta t \boldsymbol{v}(t) + \frac{1}{2}(\Delta t)^2 \boldsymbol{a}(t)\,, \tag{1}$$

$$\boldsymbol{v}(t+\Delta t) = \boldsymbol{v}(t) + \frac{1}{2}\Delta t\left[\boldsymbol{a}(t) + \boldsymbol{a}(t+\Delta t)\right], \tag{2}$$

where $\mathbf{a} = -(e/m_e)\mathbf{E}$ is the acceleration due to the electric field $\mathbf{E}$, e the elementary charge, and m_e is the electron mass.

Electron–neutral collisions are treated using the null-collision method [55] assuming isotropic scattering, with collision rates derived from cross sections, see section 2.2.1. We only consider electron–neutral collisions since the ionization degree of the discharges is typically below 10^{-4}.

2.1.2. Super-particles. In the PIC-MCC model, the stochastic development of discharges can be effectively captured by tracking individual electrons' trajectories and interactions. However, it is computationally infeasible to simulate every electron individually due to the large number of

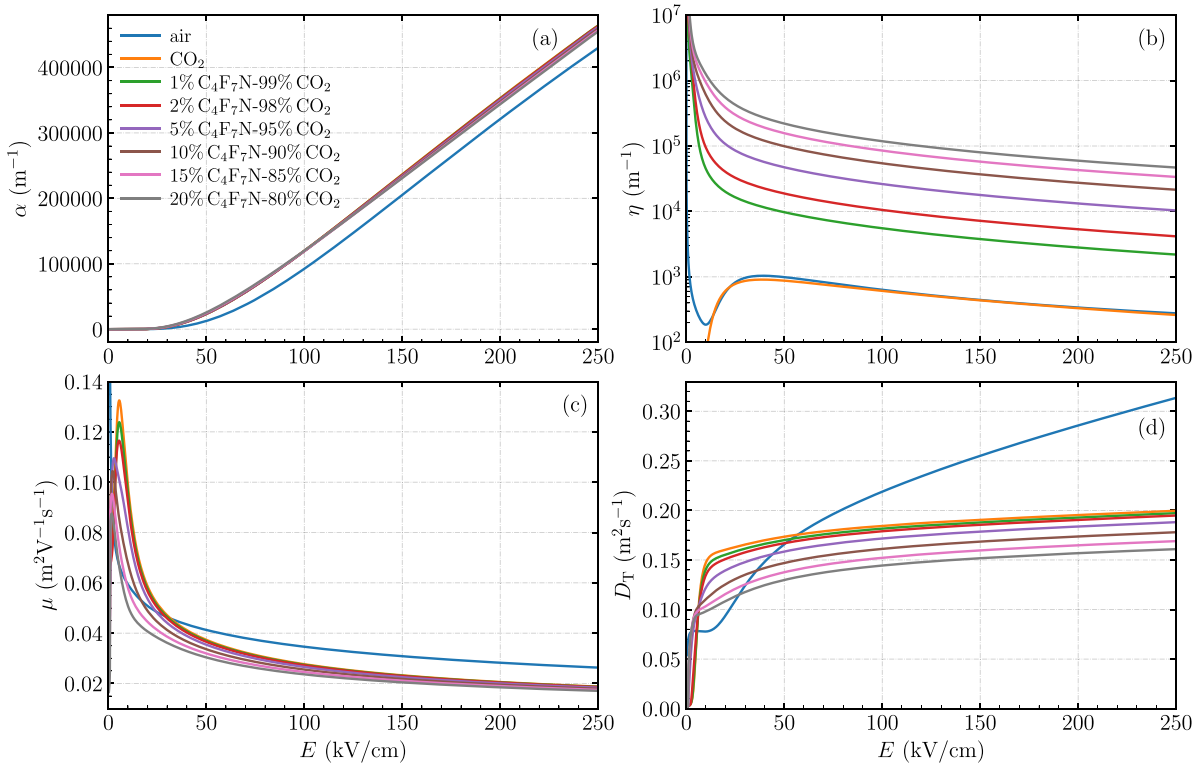

Figure 2. Comparison of electron transport data in air, pure CO_2 and C_4F_7N-CO_2 mixtures. (a) Ionization coefficient α, (b) attachment coefficient η, (c) flux mobility μ and (d) flux transverse diffusion coefficient D_T. These coefficients were computed with BOLSIG+ [63] at 300 K and 1 bar, with cross sections for artificial dry air (80% N_2 and 20% O_2) obtained from the Phelps database [62], cross sections for CO_2 obtained from the IST-Lisbon database [60], and cross sections for C_4F_7N obtained from the XJTUAETLab database [59].

electrons (above 10^8) in a typical discharge. To address this, super-particles are used, with their weights w ($w \geqslant 1$) determining the number of physical electrons they represent. Such super-particles can be merged or split between time steps using adaptive particle management [56], thereby adjusting their weights w to a desired weight w_d as

$$w_d = n_e \Delta V / N_{ppc}\,, \tag{3}$$

where n_e is the electron density in a grid cell, ΔV the cell volume, and N_{ppc} is the desired number of particles per cell, which is here set to $N_{ppc} = 100$.

Therefore, super-particles at low electron densities represent few (or even single) physical electrons, whereas those at high electron densities represent multiple physical electrons.

2.1.3. Adaptive mesh refinement for the electric field. Simulation particles are mapped to grid densities using a standard bilinear (2D) or trilinear (3D) weighting scheme. Near refinement boundaries, the mapping is locally switched to the 'nearest grid point' scheme, to maintain the conservation of particle densities [53].

Subsequently, the electric field $\mathbf{E}$ is calculated as $\mathbf{E} = -\nabla\phi$. The electric potential ϕ is obtained by solving Poisson's equation

$$\nabla^2\phi = -\rho/\varepsilon_0\,, \tag{4}$$

where ρ is the space charge density and ε_0 is the vacuum permittivity. Equation (4) is solved using the geometric multigrid method included in the Afivo library [57, 58]. The calculated electric field is then interpolated from the grid back to particles using standard bilinear or trilinear interpolation.

For computational efficiency, the `Afivo-pic` code includes adaptive mesh refinement. The mesh is refined if

$$\alpha_{eff}(E)\,\Delta x > 1\,,$$

where Δx is the grid spacing and $\alpha_{eff}(E) = \alpha(E) - \eta(E)$ is the field-dependent effective ionization coefficient, see figure 2. The minimal grid spacing is less than 1 μm in the simulations. Note that we here use the effective ionization coefficient $\alpha_{eff}(E)$ instead of the ionization coefficient $\alpha(E)$ utilized previously in [52, 53].

2.2. Input data

2.2.1. Cross sections. We use cross sections for elastic, vibrational excitation, electronic excitation, ionization and attachment collisions for C_4F_7N from the XJTUAETLab database [50, 59], as shown in figure 1. This database provides a complete cross section set for C_4F_7N.

Electron-neutral collision cross sections for CO_2 were obtained from the IST-Lisbon database [60]. This database includes an effective momentum-transfer cross section, considering both elastic and inelastic processes [61]. For PIC

Table 1. The critical electric field E_k for different gases at 300 K and 1 bar, corresponding to figure 2.

Gas	Critical electric field E_k
Air	28.2 kV cm^{-1}
CO_2	22.5 kV cm^{-1}
1% C_4F_7N-99% CO_2	40.2 kV cm^{-1}
2% C_4F_7N-98% CO_2	47.2 kV cm^{-1}
5% C_4F_7N-95% CO_2	61.0 kV cm^{-1}
10% C_4F_7N-90% CO_2	76.4 kV cm^{-1}
15% C_4F_7N-85% CO_2	88.6 kV cm^{-1}
20% C_4F_7N-80% CO_2	99.7 kV cm^{-1}

simulations, an estimated elastic cross section was obtained by subtracting the total inelastic cross sections.

For comparison of electron transport data in different gases, electron–neutral collision cross sections for air were taken from the Phelps database [62].

2.2.2. Electron transport data. Differences in electron transport data for various C_4F_7N–CO_2 mixtures, pure CO_2 and air are illustrated in figure 2. These transport coefficients were computed with BOLSIG+ [63] at 300 K and 1 bar, using cross sections described in section 2.2.1. We remark that in the PIC-MCC model, these transport coefficients are not used since electron–neutral collisions are directly determined by cross sections.

Figure 2 shows that the ionization coefficient α, flux mobility μ and flux transverse diffusion coefficient D_T are similar between these different gases. However, the attachment coefficients η in C_4F_7N–CO_2 mixtures are several orders of magnitude higher than those in pure CO_2 and air, leading to higher critical electric fields E_k (where the ionization coefficient α is equal to the attachment coefficient μ), as summarized in table 1.

2.3. 3D computational domain

We simulate negative and positive streamers in C_4F_7N–CO_2 mixtures at 300 K and 1 bar using the 3D computational domain illustrated in figure 3(a), which measures 5 mm × 5 mm × 10 mm. The domain has a plate–plate geometry with a centrally positioned electrode protruding from the upper plate. The electrode is rod-shaped with a semi-spherical tip, measuring 2 mm in length and 0.4 mm in diameter.

For the electric potential, a constant high voltage V is applied on the upper plate and the rod electrode, the lower plate is grounded, and homogeneous Neumann boundary conditions are applied on the other sides of the domain. Simulation particles are removed from the simulation if they enter the electrode or move beyond the domain boundaries. Secondary electron emission from the electrode is not included.

The axial electric field $E_{ax}(z)$ away from the rod electrode relaxes to the average field between the two plate electrodes, see figure 4. We therefore define the background electric field E_{bg} as

$$E_{bg} = |V|/d_{plates}\,, \tag{5}$$

where $d_{plates} = 10$ mm is the distance between the two plate electrodes. Note that $E_{ax}(z) \approx E_{bg}$ in most of the domain. In addition, there is the average electric field E_{avg} between the needle tip and the grounded electrode (as used in e.g. [64, 65]):

$$E_{avg} = |V|/d_{gap}\,, \tag{6}$$

where $d_{gap} = 8$ mm. In our simulations we therefore have $E_{avg} = 1.25E_{bg}$.

Note that the computational domain is relatively narrow. Since we use Neumann boundary conditions for the electric potential, the discharge will develop as if identical discharges were developing around it, by mirroring the computational domain in the x and y directions. This tends to somewhat artificially confine the discharge in the x and y directions. However, we opted for such a domain since it reduces the rather high computational costs of the simulations.

2.4. 2D computational domain

As will be discussed in section 4.1, we are only able to simulate the early inception stage of positive discharges in 3D. To qualitatively illustrate how such positive discharges could develop, we perform 2D Cartesian simulations using the computational domain shown in figure 3(b). This domain measures $(10\text{ mm})^2$ and has the same electrode geometry and boundary conditions as the 3D domain discussed above.

2.5. Included free electron sources

In the simulations, we consider two sources of (initial) free electrons: a plasma seed near the electrode tip or stochastic background ionization, which will be explained below. With a plasma seed, we are able to start negative discharges that continue to propagate, but not positive ones. Positive discharges require a source of free electrons ahead of them for their propagation, but there is considerable uncertainty in the mechanisms that could provide such free electrons in C_4F_7N–CO_2 mixtures.

Two potential free electron sources are background ionization and photoionization. Due to the fast attachment of electrons to C_4F_7N, background ionization would be present in the form of positive and negative ions. Although there is evidence of electron detachment in high electric fields and low pressures in pure C_4F_7N [51], it is not yet known which ions would form in C_4F_7N–CO_2 mixtures at atmospheric pressure and how easily electrons would detach from these ions. Even less is known about photoionization in these mixtures. However, since photoionization in CO_2 is much weaker than in air, due to the lower production of ionizing photons and their significantly smaller absorption distance [66], we expect photoionization to be weak in C_4F_7N–CO_2 mixtures as well.

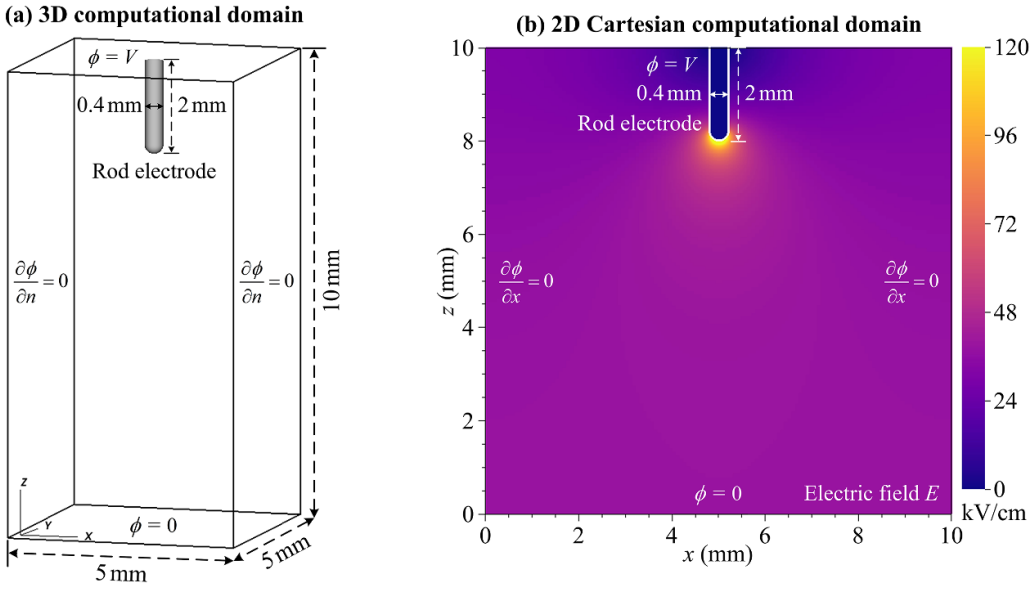

Figure 3. A view of (a) the 3D (5 mm × 5 mm × 10 mm) and (b) the 2D $(10\ \text{mm})^2$ Cartesian computational domains. Panel (b) also shows the electric field profile E without a discharge at an applied voltage $V = -36$ kV. The centrally positioned rod electrode, protruding from the upper plate, has a length of 2 mm and a diameter of 0.4 mm. Boundary conditions for the electric potential ϕ are indicated.

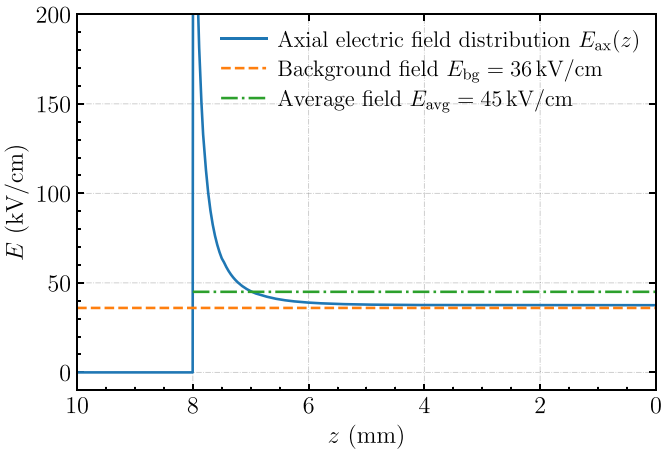

Figure 4. Axial electric field distribution $E_{ax}(z)$ without a discharge for an applied voltage $V = -36$ kV. The background electric field E_{bg} and the average electric field E_{avg} are also indicated.

Due to the above uncertainties we decided to include a simple stochastic background ionization process in some of our simulations, to qualitatively illustrate how discharges would develop with a continuous free electron source. Electron–ion pairs are produced in the whole computational domain at a rate k_0 between $10^{18}\,\text{m}^{-3}\text{s}^{-1}$ and $10^{19}\,\text{m}^{-3}\text{s}^{-1}$. Note that these amounts correspond to $1\,\text{mm}^{-3}\text{ns}^{-1}$ and $10\,\text{mm}^{-3}\text{ns}^{-1}$, respectively. This production rate is high compared to laboratory experiments with a radioactive admixture [67], but much lower than the production rate of photoelectrons in air-like mixtures (for reference, in atmospheric air the photoionization rate is typically between $10^{22}\,\text{m}^{-3}\text{s}^{-1}$ and $10^{24}\,\text{m}^{-3}\text{s}^{-1}$ one millimeter away from a streamer discharge).

In the rest of our simulations (without stochastic background ionization), we only include an initial neutral seed near the tip of the electrode. Electron–ion pairs are then generated according to a Gaussian distribution as

$$n_e(\mathbf{r}) = n_i^+(\mathbf{r}) = N_0 \exp\left[-\frac{(\mathbf{r}-\mathbf{r}_0)^2}{\sigma^2}\right], \qquad (7)$$

where $N_0 = 2\times10^{11}\,\text{m}^{-3}$ (unless specified otherwise), $\sigma = 0.2$ mm, and $\mathbf{r}_0$ is the position of the electrode tip located at $z = 8$ mm. The expected number of electrons in such a seed is $\pi^{3/2}\sigma^3 N_0$, which is about 9 with the above values.

3. Negative streamers in C_4F_7N–CO_2 mixtures

3.1. Streamers with an initial neutral seed

We first present 3D simulation results of negative streamers that start from an initial neutral seed placed near the electrode tip.

3.1.1. Effect of the background electric field. Figure 5 illustrates the effect of the background electric field E_{bg} on negative streamers in a 1% C_4F_7N-99% CO_2 mixture. First, in figure 5(b) we look into the case of a background field of $E_{bg} = 36\,\text{kV cm}^{-1}$, which corresponds to $E_{avg} = 45\,\text{kV cm}^{-1}$. For comparison, the critical field E_k is about $40\,\text{kV cm}^{-1}$. At $t = 1$ ns, electrons provided by the initial neutral seed initiate a streamer near the electrode due to the locally high electric field. The negative discharge grows at an almost constant velocity of about $0.5\times10^6\,\text{m s}^{-1}$ until it crosses the gap at $t = 19$ ns. Multiple branches form during its propagation.

Electrons are primarily observed around the streamer head, where the maximal electron density is about $10^{20}\,\text{m}^{-3}$, as those inside the streamer channel rapidly attach to C_4F_7N. Only a short part of the channel behind the streamer head therefore

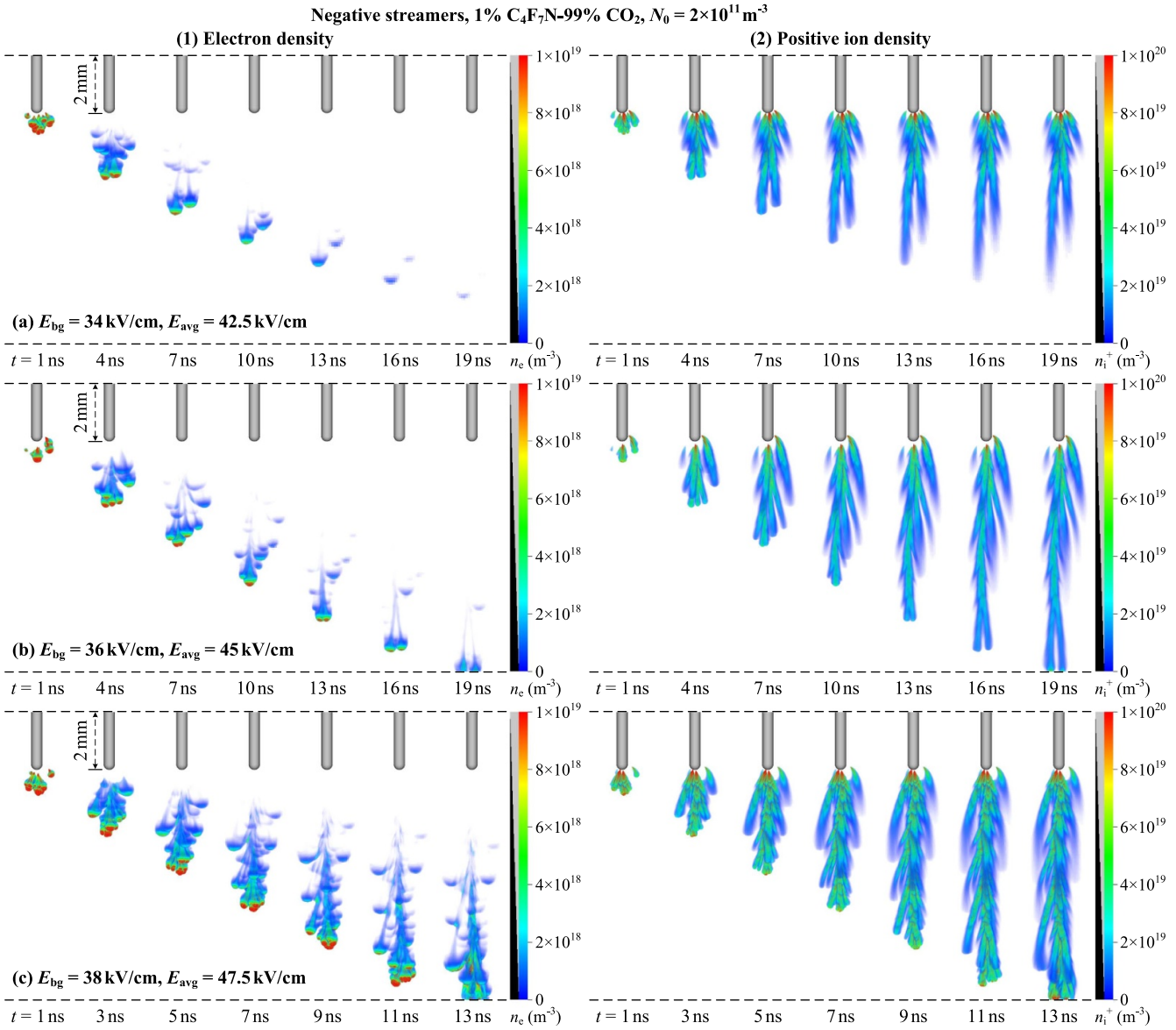

Figure 5. Effect of the background electric field E_{bg} on the propagation of negative streamers in a 1% C_4F_7N-99% CO_2 mixture with an initial neutral seed using 3D simulations. The upper and lower plate electrodes are here and afterward respectively indicated by a dashed line. Shown is the time evolution of (1) the electron density n_e and (2) the positive ion density n_i^+ through Visit's [68] 3D volume rendering; the opacity is indicated in the legend. The same visualization is also applied to subsequent 3D simulations. A short conductive channel is observed behind the streamer head due to the fast attachment of electrons to C_4F_7N, so that the background field required to cross the gap is approximately the critical field $E_k \approx 40\,\mathrm{kV\,cm^{-1}}$. We remark that the maximal electron density is about $10^{20}\,\mathrm{m^{-3}}$, which is well above the limit of the color scale.

has a significant electron conductivity, with the electric field in the channel approximately relaxing back to the background electric field, as shown in figure 6. To better show the discharge trajectory and morphology, the positive ion density n_i^+ is also included in figure 5 as well as subsequent figures. Note that the color scale in these visualizations can affect apparent width of the channels, as illustrated in appendix A.

In figure 5(a), the background electric field is decreased to $E_{bg} = 34\,\mathrm{kV\,cm^{-1}}$, corresponding to $E_{avg} = 42.5\,\mathrm{kV\,cm^{-1}}$. The negative discharge now decelerates and fades out before reaching the lower plate, losing its field enhancement, similar to fading negative streamers in air [69]. This is initially surprising, since the average electric field $E_{avg} = 42.5\,\mathrm{kV\,cm^{-1}}$ exceeds E_k. However, this phenomenon can be explained by the fast decay of the electron conductivity in the channels, which leads to streamers with weak field enhancement and poorly conducting channels, as illustrated in figure 6. Streamers in strongly attaching gases thus modify the background electric field to a much smaller extent than streamers in gases such as air, which means that their propagation requires a background electric field close to the critical field E_k. When $E_{avg} \approx E_k$, there is a region where the background

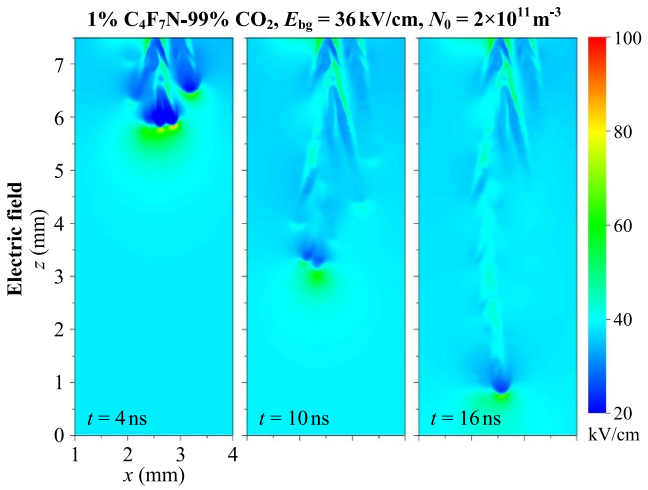

Figure 6. Cross sections of the electric field E for the negative streamer shown in figure 5(b) at $E_{bg} = 36\,\mathrm{kV\,cm^{-1}}$. The electric field behind the streamer head approximately relaxes back to the background electric field due to rapid electron attachment. Note that the color scale ranges from $20\,\mathrm{kV\,cm^{-1}}$ to $100\,\mathrm{kV\,cm^{-1}}$.

field exceeds E_k near the rod electrode but also a region below E_k farther away from it, and streamers can stop propagating in the latter region, as shown in figure 5(a).

3.1.2. Effect of the initial neutral seed. The streamers cross the gap in a background field $E_{bg} \approx 36\,\mathrm{kV\,cm^{-1}}$. This value is close to the critical field E_k, as has also been observed in the electronegative gas SF_6 [70]. The reason is that fast electron attachment shortens the conductive channel behind the streamer head, which strongly reduces the electric field enhancement at the head. (For comparison, the effect of strong attachment on axisymmetric streamers in air was studied in [71].)

From these results, one might conclude that the stability field E_{st} is $36\,\mathrm{kV\,cm^{-1}}$, if the stability field is defined as the background electric field required for a streamer to cross a gap [72]. However, we have shown recently in [69, 73] that the electric field where streamers in air propagate steadily, i.e. with constant shape and velocity, depends on their radius. So there is no unique stability field, but streamers with larger radii propagate steadily in lower background electric fields. A similar effect can be seen in figure 7. Here the same conditions are used as in figure 5(b), except that the maximal electron density N_0 of the initial seed is changed from $2 \times 10^{11}\,\mathrm{m^{-3}}$ to $1 \times 10^{11}\,\mathrm{m^{-3}}$ and $5 \times 10^{11}\,\mathrm{m^{-3}}$, respectively. Although most discharges are able to cross the gap, we find that the larger seed creates a wider discharge containing more streamer channels, making it easier for the discharge to cross the gap in the same background field of $E_{bg} = 36\,\mathrm{kV\,cm^{-1}}$. The average streamer velocity is also about 40% higher. This is due to a collective effect where neighboring branches mutually increase the electric field enhancement at the streamer head.

3.1.3. Effect of the C_4F_7N concentration. The effect of the C_4F_7N concentration is illustrated in figure 8, where the C_4F_7N fraction is increased to 5%, 10% and 20%. These mixtures are of interest in practical applications as their dielectric strength is comparable to SF_6. Given the sensitivity of negative streamer propagation to the background electric field E_{bg}, here we set $E_{bg} = 0.9\,E_k$ for all cases, see table 1.

All negative streamers decelerate and fade out before crossing the gap, in contrast to the case with 1% C_4F_7N shown in figure 5(b), which is also at $E_{bg} = 0.9\,E_k$. Furthermore, the streamer channels are thinner, slower and they branch more when the C_4F_7N fraction is increased, and they stop earlier. This indicates that for increased C_4F_7N concentrations the background electric field E_{bg} required to cross the gap is above $0.9\,E_k$, due to a higher electron attachment rate that further decreases the streamer's electric field enhancement.

3.2. Streamers with stochastic background ionization

We now perform 3D simulations of negative streamers in which the initial neutral seed is replaced by stochastic background ionization that continuously produces electron–ion pairs within the computational domain, as discussed in section 2.5. Although such background ionization is not required for negative streamer propagation, we do observe some interesting effects in figure 9, in which the background ionization rate k_0 is varied. With a higher k_0 more electron–ion pairs are produced per unit of time. As expected, this results in earlier initiation and the formation of a greater number of streamers.

A remarkable phenomenon is that new negative streamers are generated behind the previous ones. This happens because the electric field behind previous streamers quickly relaxes back to the background electric field, due to rapid electron attachment, which allows new streamers to form. This process repeats itself, at least within the time scales considered, so that a chain of negative streamers emerges. In some cases, later streamers are faster and they can approach or overtake previous ones, as shown in figure 9(a) for the streamers numbered (2) and (3). Although there is only a low electron conductivity behind the repeated streamers, the ion density and hence the ion conductivity increase over time, if the recombination of positive and negative ions is not too fast. If the ion conductivity keeps increasing, we expect that the ions eventually will screen the electric field and inhibit the formation of new streamers.

4. Positive streamers in C_4F_7N–CO_2 mixtures

In this section, we perform both 3D and 2D simulations of positive streamers in C_4F_7N–CO_2 mixtures. The simulations include stochastic background ionization, which serves as the source of free electrons for positive streamer propagation, as discussed in section 2.5.

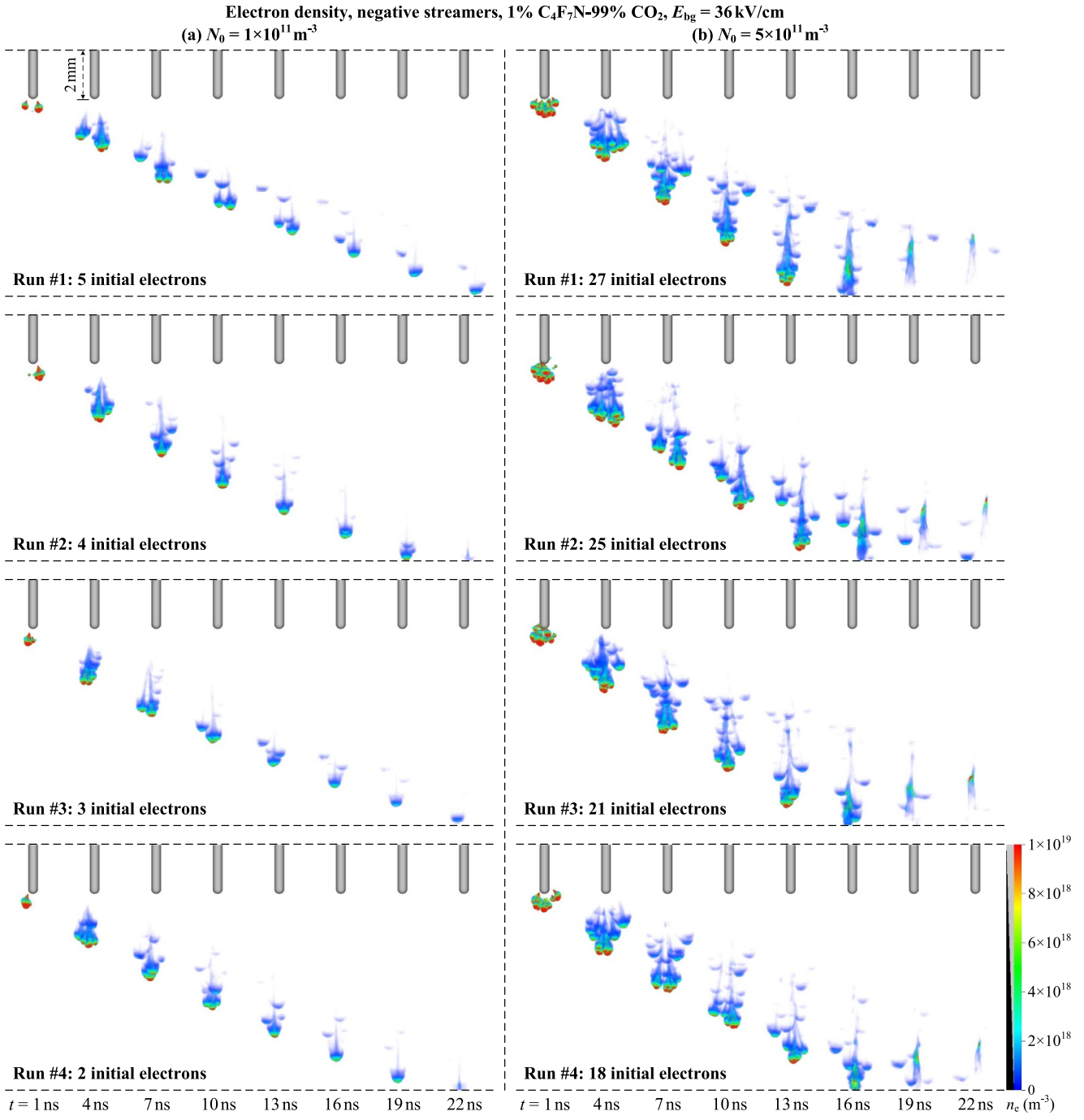

Figure 7. Effect of the maximal electron density N_0 of the initial seed on the propagation of negative streamers. All parameters are the same as in figure 5(b), except for N_0, which is changed from $2 \times 10^{11}\,\mathrm{m}^{-3}$ to $1 \times 10^{11}\,\mathrm{m}^{-3}$ and $5 \times 10^{11}\,\mathrm{m}^{-3}$, respectively. For both cases, four simulation runs with different numbers of initial electrons are shown. An increase of the density N_0 leads to the formation of a wider and faster discharge containing more streamer channels, making it easier for the discharge to cross the gap. This resembles the observation that in air streamers with larger radii propagate steadily in lower background fields [69, 73].

4.1. 3D simulation results

In 3D, we can only simulate the early inception stage of positive discharges. Two examples for $k_0 = 1 \times 10^{19}\,\mathrm{m}^{-3}\mathrm{s}^{-1}$ and $k_0 = 5 \times 10^{19}\,\mathrm{m}^{-3}\mathrm{s}^{-1}$ are shown in figure 10. In these simulations, electron avalanches develop towards the electrode, which quickly transition into negative streamers. Since these negative streamers are much thinner than the electrode itself, the maximal electric field at the streamer heads becomes extremely high, exceeding $10^8\,\mathrm{V\,m}^{-1}$, as illustrated

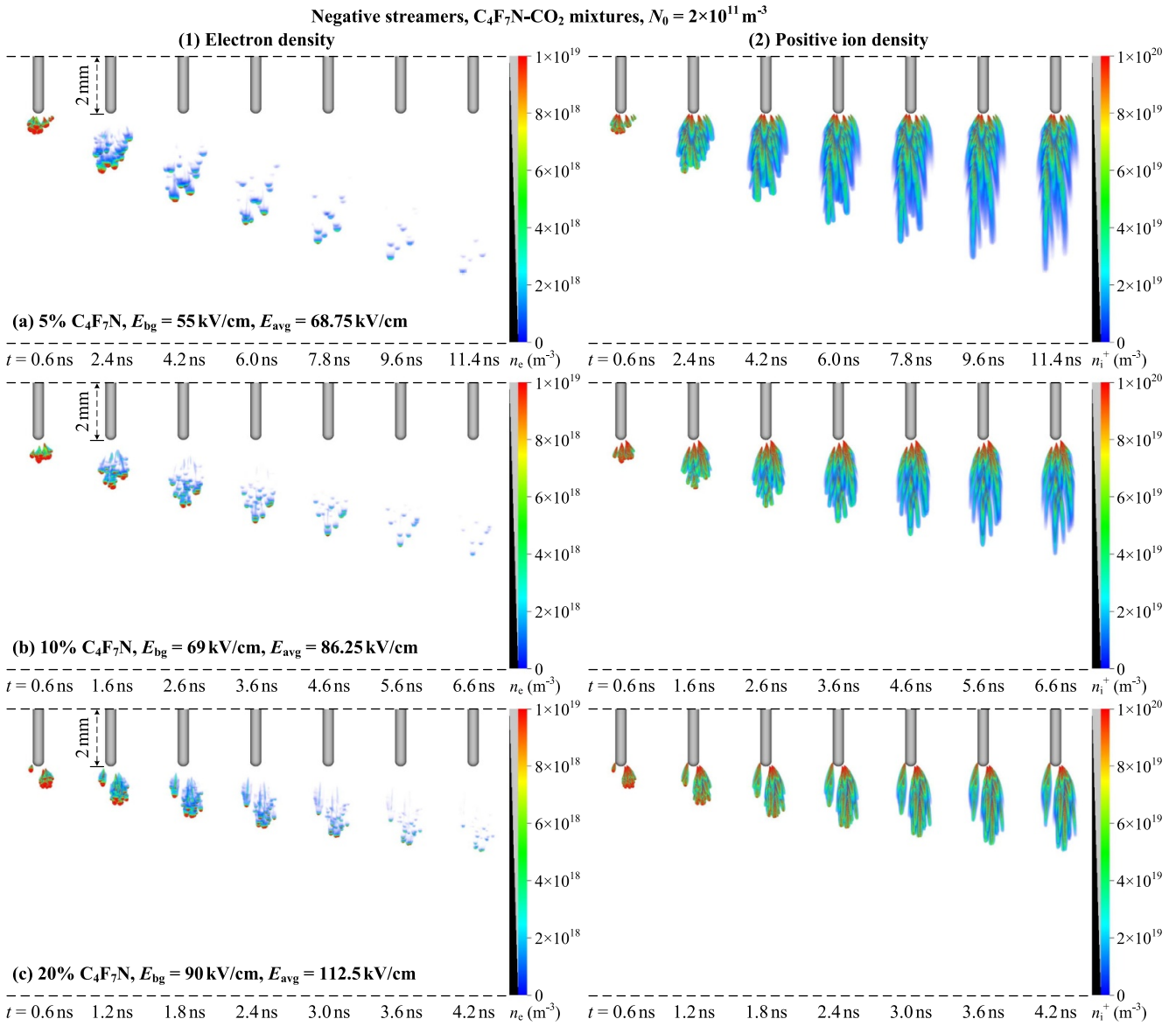

Figure 8. Effect of the C_4F_7N concentration on the propagation of negative streamers at $E_{bg} = 0.9\,E_k$ with an initial neutral seed, see table 1. The maximal electron density is about $10^{21}\,m^{-3}$. As the C_4F_7N concentration increases, the streamer branches into more channels, which are thinner, slower, and stop earlier.

in figure 11. This also results in very high electron densities, exceeding $10^{23}\,m^{-3}$.

Computationally, it is very demanding to simulate discharges with such high fields and electron densities, due to the high grid resolution (below 1 μm) and small time steps (below 10^{-14} s) required. Although we are only able to simulate the first stages of inception, our results suggest that positive discharges develop in a highly irregular way in C_4F_7N–CO_2 mixtures, with sharp features and very high fields at their tips. We speculate that the growth of positive discharges will be the result of incoming negative streamers that connect to an existing discharge channel. To qualitatively study such growth, we will perform 2D Cartesian simulations in section 4.2.

4.2. 2D Cartesian simulation results

To qualitatively study the growth of positive discharges in C_4F_7N–CO_2 mixtures, we now perform 2D Cartesian simulations. Computational costs are much lower in such a geometry, not only because there is one less dimension but also because field enhancement is significantly weaker, as there is no curvature in the third dimension. Although there are quantitative differences between 2D and 3D in terms of streamer properties and branching, 2D simulations can help to qualitatively understand the growth of positive discharges.

The interpretation of particle weights and stochastic fluctuations is somewhat complicated in 2D. We here use a

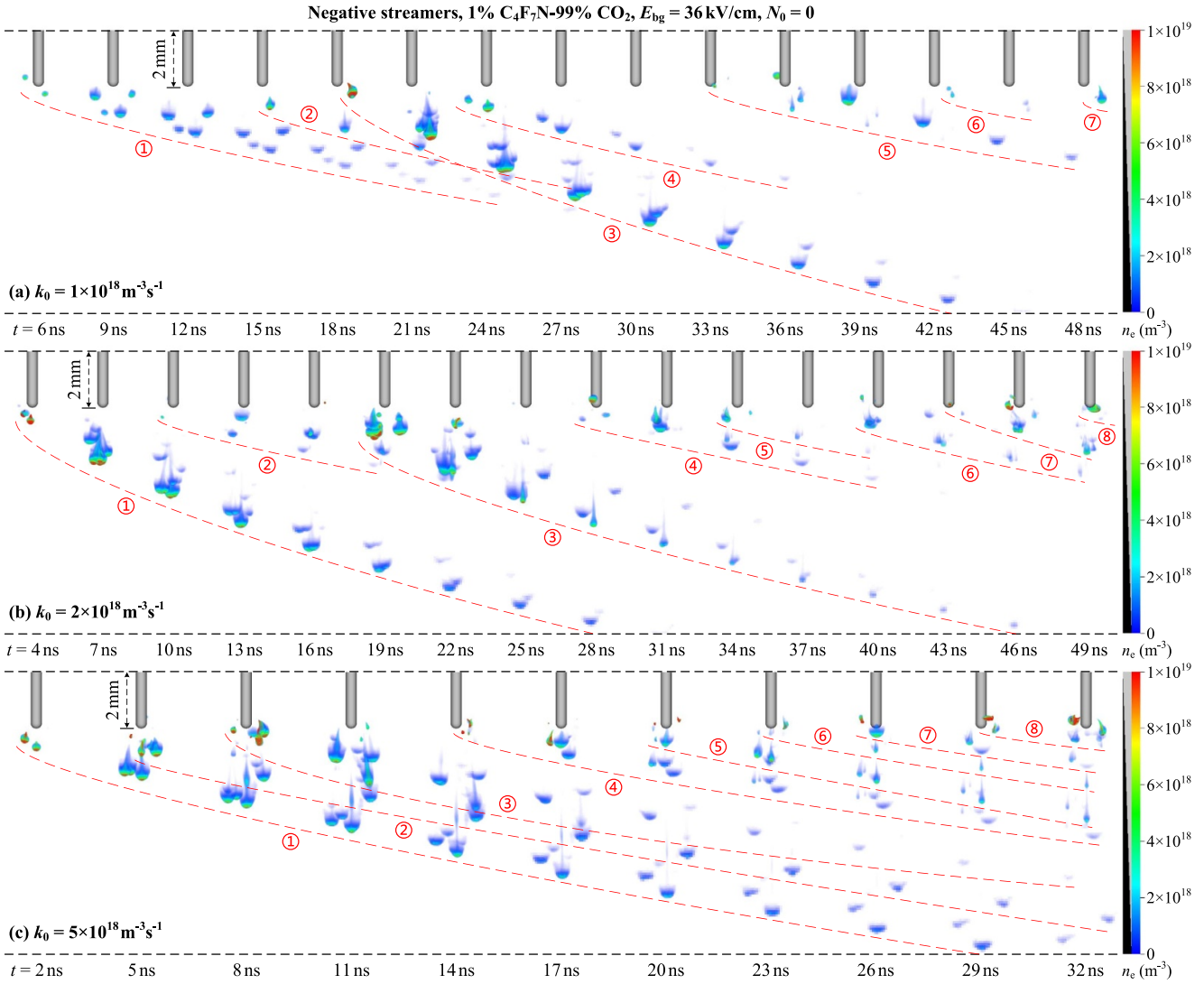

Figure 9. Effect of the background ionization rate k_0 on the propagation of negative streamers without an initial neutral seed. The maximal electron density is about $10^{20}\,\mathrm{m}^{-3}$. With stochastic background ionization, a remarkable phenomenon occurs where new negative streamers are generated behind the previous ones, due to rapid electron attachment. This process repeats itself leading to the formation of a chain of negative streamers, each represented by a red dashed curve and sequentially numbered to indicate their order of emergence.

minimum particle weight of $w_{\min} = 10^5\,\mathrm{m}^{-1}$. This can for example be interpreted as having an unresolved 'third' dimension in the simulations of 1 m and a minimum particle weight of 10^5, or equivalently as having and a third dimension of $10\,\mu$m and a minimum weight of one, see [74] for details. We will express the background ionization rate as $k_0/w_{\min}$, with units $\mathrm{m}^{-2}\mathrm{s}^{-1}$.

Figure 12 shows the time evolution of a positive streamer in a 1% C_4F_7N-99% CO_2 mixture with $E_{\mathrm{bg}} = 36\,\mathrm{kV\,cm}^{-1}$ ($E_{\mathrm{avg}} = 45\,\mathrm{kV\,cm}^{-1}$) and $k_0/w_{\min} = 1 \times 10^{14}\,\mathrm{m}^{-2}\mathrm{s}^{-1}$. Electron avalanches form due to stochastic background ionization, and they initially develop towards the electrode from various directions. During their development, these avalanches transition into short negative streamers, which connect to each other, thereby extending the positive streamer channel. This process repeats over time, leading to the irregular and branched downward propagation of the positive streamer.

In figure 13 we present eight different positive streamers by varying the background electric field E_{bg}, background ionization rate $k_0/w_{\min}$ and C_4F_7N concentration. Results are shown at $t = 50$ ns, and the streamers in panels (d)–(h) have crossed the gap. In all cases, the positive channels extend by incoming negative streamers, as was illustrated by the temporal evolution in figure 12. Note that the number of streamer channels increases with the background field and with the background ionization rate.

In 3D, we expect positive streamers to grow in a similar manner, with the channels extending by incoming negative streamers. However, the electric fields at the streamer tips

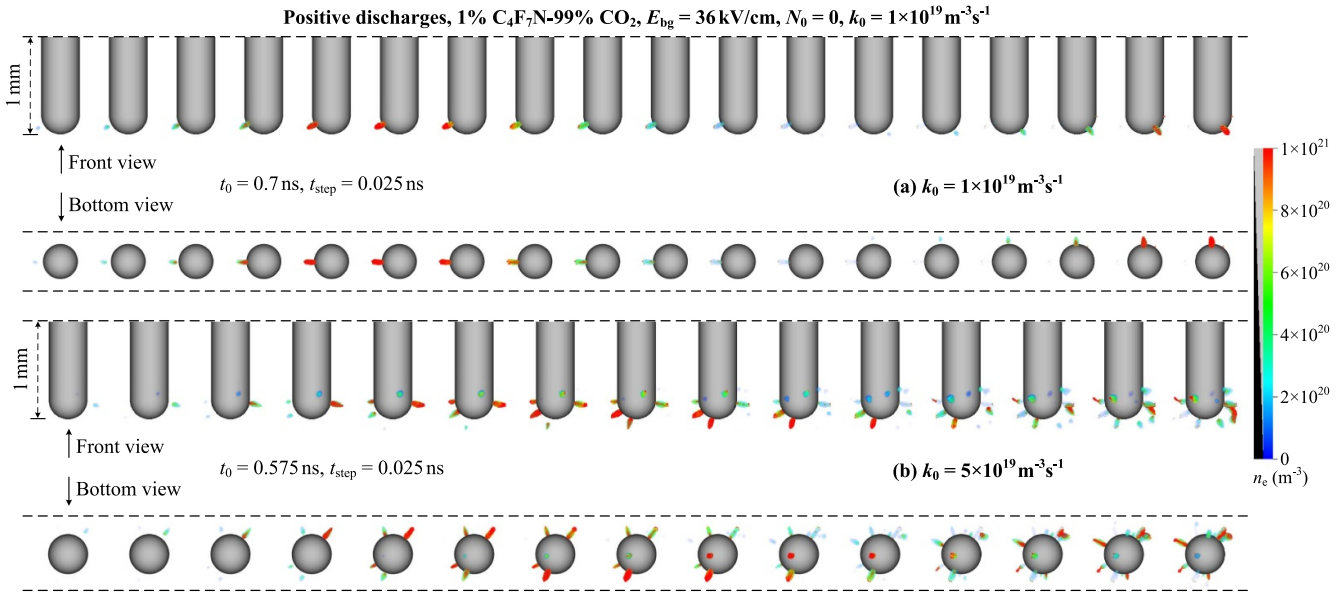

Figure 10. Two examples of positive discharges in 3D simulations using stochastic background ionization, without an initial neutral seed. Both the side and bottom views are presented, with a zoomed-in perspective centered at the electrode tip. Here we only show the time evolution of the electron density n_e in time steps of 0.025 ns through Visit's 3D volume rendering, with a linear scale ranging from 0 to $1 \times 10^{21}\,\mathrm{m}^{-3}$. The maximal electron density is about $10^{24}\,\mathrm{m}^{-3}$. In 3D, we are only able to simulate the early inception stage of positive discharges due to the presence of extremely high electric fields and electron densities.

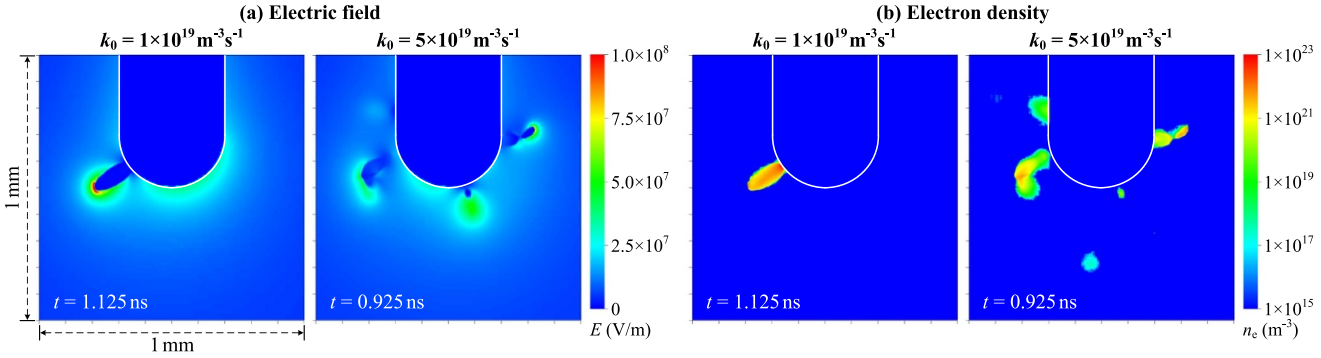

Figure 11. Cross sections of (a) the electric field E and (b) the electron density n_e for the two positive discharges shown in figure 10 at the last frame, with a $(1\,\mathrm{mm})^2$ zoomed-in perspective centered at the electrode tip. Note that n_e is shown on a logarithmic scale. E_{max} exceeds $10^8\,\mathrm{V\,m}^{-1}$, and the maximal electron density exceeds $10^{23}\,\mathrm{m}^{-3}$.

would be much higher, and so would be the electron densities. Furthermore, one would generally expect more branching in 3D, although the number of branches would to some extent depend on the amount of background ionization. Such highly stochastic growth has been experimentally observed in gases with weak or no photoionization [75].

5. Comparison with past computational work

Below, we briefly discuss related computational work. To the best of our knowledge, all previous simulations of discharges in C_4F_7N mixtures were performed using 2D fluid models. In [36], streamers in C_4F_7N mixtures with different buffer gases were simulated at 300 K and 1 bar using an axisymmetric model [76]. Both ionization and attachment processes were considered, with their coefficients interpolated from [16, 19, 77]. Photoionization was not considered, but instead an initial homogeneous density of $10^{14}\,\mathrm{m}^{-3}$ for electrons and positive ions was included. The results showed that a higher background field was required for streamers to propagate in C_4F_7N–N_2 than in C_4F_7N–CO_2.

In [38], negative corona discharges in C_4F_7N–N_2 and C_4F_7N–CO_2 mixtures were simulated at 300 K and 4 bar using an axisymmetric model. The ionization and attachment cross sections of C_4F_7N were obtained from [16, 45], respectively. Electron–ion and ion–ion recombination processes were also considered. The negative corona discharges started from an initial Gaussian seed, and no other background ionization was included. However, most of the negative discharges in the

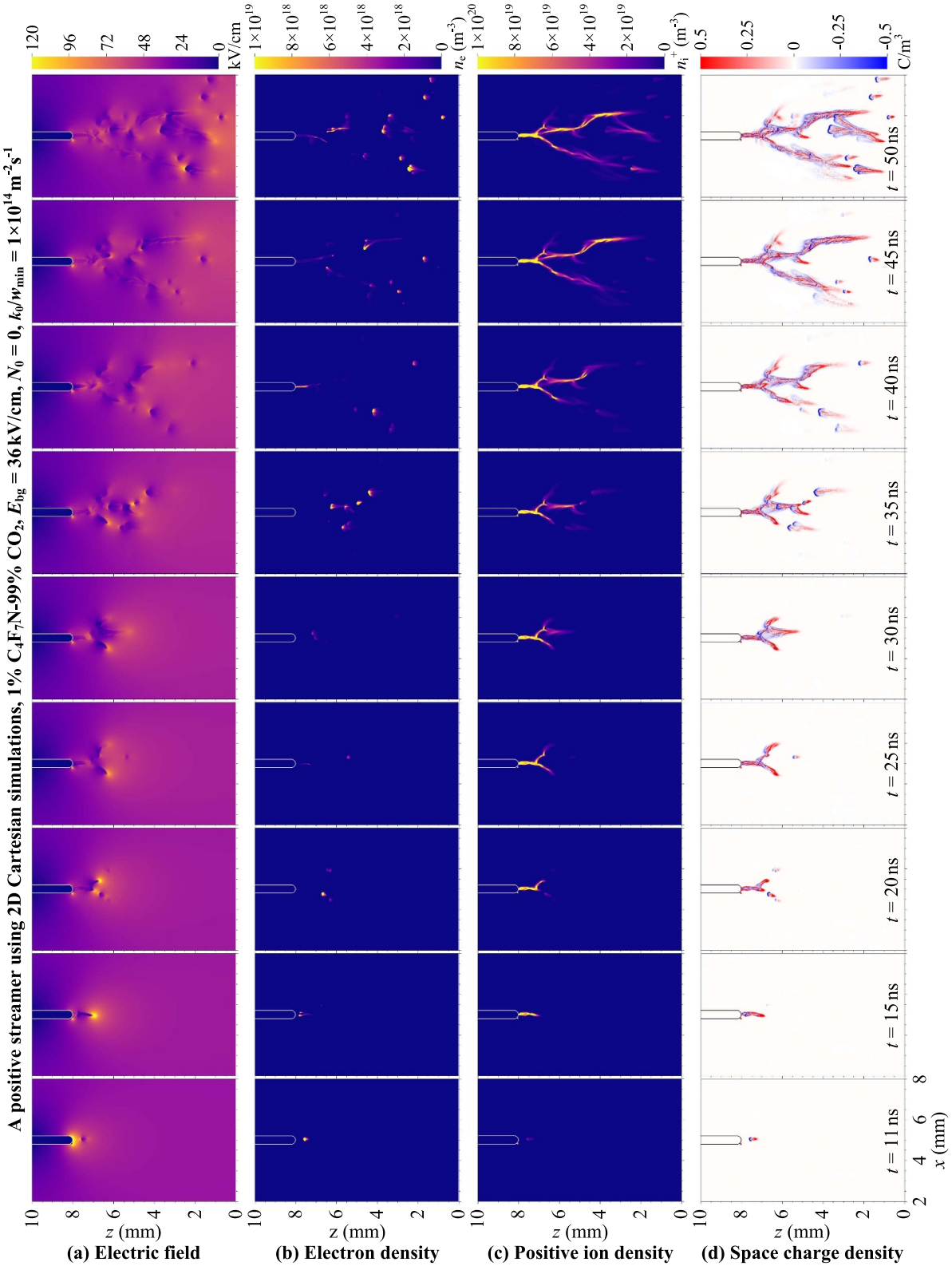

Figure 12. An example of a positive streamer using 2D Cartesian simulations with a background ionization rate $k_0/w_{\min} = 1 \times 10^{14}\,\mathrm{m^{-2}s^{-1}}$, without an initial neutral seed. Shown is the time evolution of (a) the electric field E, (b) the electron density n_e, (c) the positive ion density n_i^+ and (d) the space charge density ρ. The growth of the positive discharge exhibits a highly irregular and branched structure, resulting from incoming negative streamers that connect to existing channels.

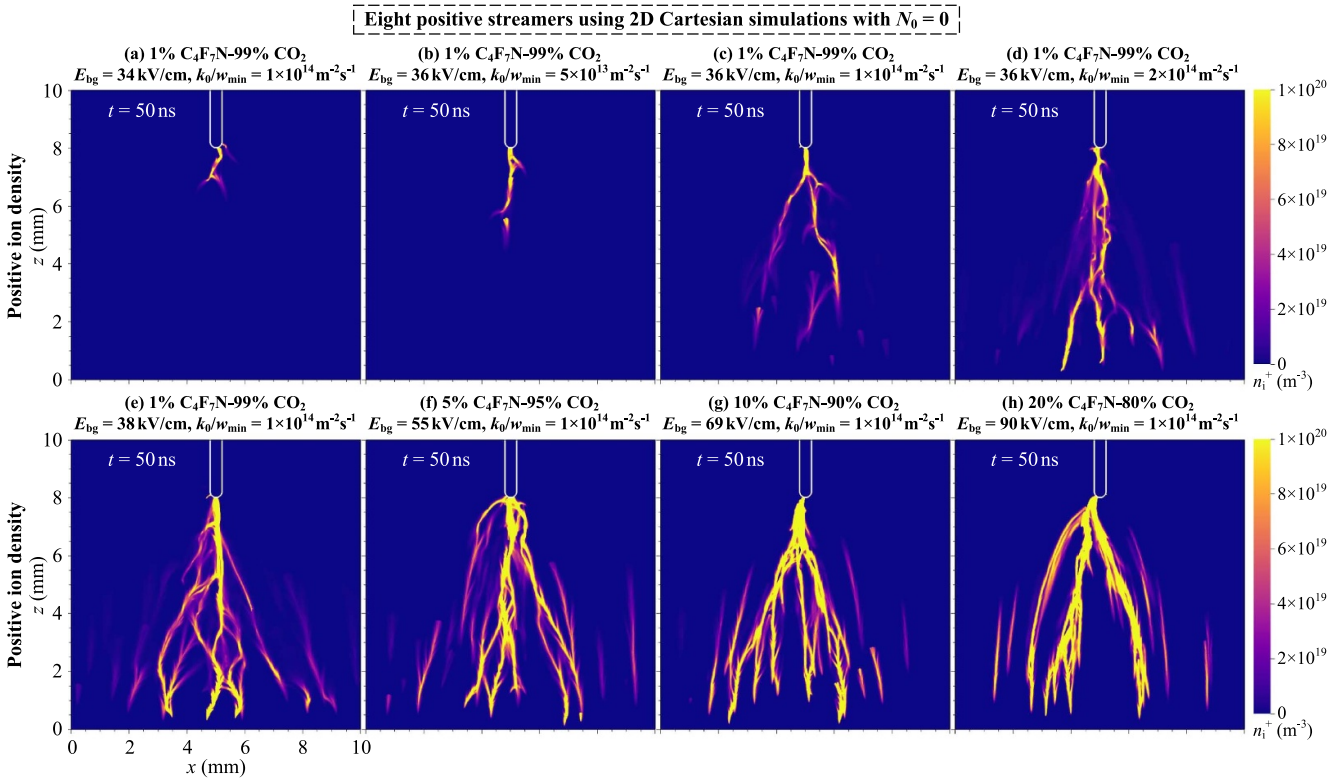

Figure 13. Positive ion density n_i^+ for eight different positive streamers at $t = 50$ ns using 2D Cartesian simulations with stochastic background ionization, without an initial neutral seed. The background electric field E_{bg}, background ionization rate k_0/w_{min} and C_4F_7N concentration are varied. All the positive streamers develop in a highly irregular way, with the positive channels extending by incoming negative streamers.

simulations remained in the inception stage and were far from propagation.

In [39], positive streamers in C_4F_7N were simulated in 2D with varying electrode shapes, using the same cross section data as [49]. An unspecified background ionization density was assumed as a replacement for photoionization. Increasing the applied voltage led to higher maximum electric fields and velocities. In another study [40], the authors performed 2D simulations of surface discharges in a 9% C_4F_7N-91% CO_2 mixture at 300 K and 1 bar, again using an unspecified background ionization density. They investigated the effect of the applied voltage and the dielectric constant on the discharge, and compared surface discharges in C_4F_7N–CO_2 with those in SF_6.

The main novelty of our work is that we for the first time use 3D particle simulations, with which we can capture the stochastic inception and branching of streamers in C_4F_7N–CO_2 mixtures. These stochastic aspects are particularly important since these mixtures appear to lack an effective photoionization mechanism, which results in much more irregular discharge growth than for example in air.

Another difference is that we have included a stochastic background ionization process in some of the simulations, which produces electron–ion pairs at a certain rate over time. In previous simulations of positive discharges, an initial background ionization density was assumed. We observed that an initial electron density would quickly decay due to rapid attachment (unless the background field E_{bg} was above the critical field E_k), after which positive streamer propagation was hardly possible. However, both approaches are rather artificial, and further work is necessary to better understand free electron sources in such mixtures, such as photoionization and electron detachment from negative ions.

Our observation that streamers in C_4F_7N–CO_2 mixtures can only keep propagating if the background electric field E_{bg} is approximately the critical electric field E_k (due to rapid electron attachment) is in agreement with previous work. However, the observed discharge growth in our 3D simulations differs significantly from that observed in previous 2D fluid simulations. First, we observe stochastic growth with frequent branching, both for negative and positive polarities. Second, we observe that new negative streamers can form behind previous ones, forming a chain of negative streamers. Third, in 2D Cartesian simulations we see that positive discharges extend due to incoming negative streamers that connect to existing channels.

6. Conclusions and outlook

We have simulated negative and positive streamers in C_4F_7N–CO_2 mixtures at 300 K and 1 bar, using a 3D and 2D PIC

model. Negative streamers were able to start from a small number of initial electrons near an electrode, whereas positive streamers required a sustained source of free electrons ahead of them for their propagation. We included an artificial stochastic background ionization process to provide such free electrons.

For negative streamers, a short conductive channel was observed behind the streamer head due to the fast attachment of electrons to C_4F_7N. Due to the short channel, these discharges did not gain as much field enhancement as streamers in most other gases, so the background field required for streamer propagation was approximately the critical electric field. Surprisingly, new negative streamers could be generated behind the previous ones when a stochastic background ionization process was included. In this manner a chain of negative streamers could form.

Simulating positive streamers required the inclusion of the artificial background ionization process, and it was much more challenging due to the presence of extremely high fields and electron densities. In 3D, we were only able to simulate the early inception stage of positive discharges. To qualitatively investigate the growth of these discharges, we performed 2D Cartesian simulations. We observed that positive discharge growth resulted from incoming negative streamers that connected to existing channels. This led to highly irregular discharge growth, in which branching was determined by the locations of free electrons ahead of the discharge.

If there is indeed no effective photoionization mechanism in C_4F_7N–CO_2 mixtures, our results suggest that negative streamers will propagate more easily than positive ones. This is in contrast to the behavior in air, where positive streamers initiate and propagate more easily than negative streamers [78, 79].

Outlook. A better understanding of free electron sources such as photoionization and electron detachment is important for the modeling of streamer-like discharges in C_4F_7N–CO_2 mixtures. Including ion kinetics could also be important, as was demonstrated in [51]. It would be valuable if streamer propagation could be captured experimentally, so that simulations and experiments could directly be compared. Furthermore, a novel type of simulation model might be required to study positive discharges in these mixtures, because 3D simulations are currently too expensive due to the complex discharge structure and the extremely high electric fields and electron densities.

Finally, it would be interesting to consider additional ionization mechanisms. First, future research could include secondary electron emission due to ions to more realistically study the inception of negative streamers, as in e.g. [80]. Second, when the fraction of C_4F_7N or the pressure is increased together with the applied electric field, it could be interesting to include field ionization as in e.g. [81].

Data availability statement

The data that support the findings of this study are openly available at the following URL/DOI: https://doi.org/10.5281/zenodo.8214598.

Acknowledgments

B G was funded by the China Scholarship Council (CSC) (Grant No. 201906280436). We thank Prof. Dr Christian Franck from Swiss Federal Institute of Technology and Prof. Dr Bobby Antony from Indian Institute of Technology for sharing cross section data for C_4F_7N, and we thank Dr Bastiaan Braams at CWI for valuable discussions.

Appendix A. Effect of the color scale on streamer visualization

Figure A1 presents results with different color scales for negative streamers shown in figure 5(b) at $t = 10$ ns, with the maximum scale value being $1 \times 10^{19}\,\mathrm{m}^{-3}$, $5 \times 10^{19}\,\mathrm{m}^{-3}$ and $1 \times 10^{20}\,\mathrm{m}^{-3}$, respectively. With a higher value of the maximum, the streamers appear to be thinner.

Throughout the paper, a linear scale ranging from 0 to $1 \times 10^{19}\,\mathrm{m}^{-3}$ is used for the electron density n_e and a linear scale ranging from 0 to $1 \times 10^{20}\,\mathrm{m}^{-3}$ is used for the positive ion density n_i^+, except for the 3D simulations of positive discharges shown in section 4.1, which have much higher densities, see figures 10 and 11.

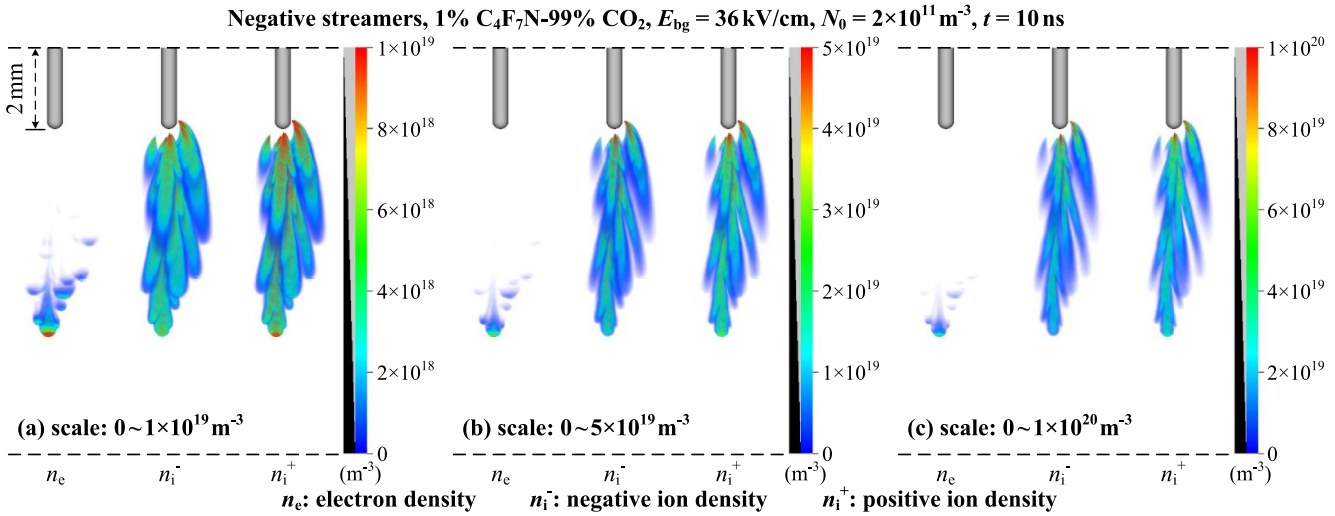

Figure A1. The case of negative streamers in figure 5(b) at $t = 10$ ns. Shown is the electron density n_e, negative ion density n_i^- and positive ion density n_i^+ through Visit's 3D volume rendering with different color scales. With a higher maximum value of the color scale streamer channels appear to be thinner.

Appendix B. Computational costs

The primary drawback of a 3D PIC-MCC model is its high computational cost, due to the large number of simulation particles required. The simulations in this paper were performed on workstations with 8 cores and 32–64 GB of RAM, using at most 5×10^8 simulation particles. The run time for the negative cases shown in section 3 was about 1 week, whereas the 3D simulations of positive streamer inception shown in section 4.1 took about 2 weeks. The 2D simulations of positive streamers shown in section 4.2 only took a few hours.

ORCID iDs

Baohong Guo https://orcid.org/0000-0001-8368-5014
Ute Ebert https://orcid.org/0000-0003-3891-6869
Jannis Teunissen https://orcid.org/0000-0003-0811-5091

References

[1] Christophorou L G, Olthoff J K and Van Brunt R J 1997 Sulfur hexafluoride and the electric power industry *IEEE Electr. Insul. Mag.* **13** 20–24
[2] Malik N H and Qureshi A H 1978 Breakdown mechanisms in sulphur-hexafluoride *IEEE Trans. Electr. Insul.* **EI-13** 135–45
[3] Boggs S A and Schramm H-H 1990 Current interruption and switching in sulphur hexafluoride *IEEE Electr. Insul. Mag.* **6** 12–17
[4] Ray E A, Moore F L, Elkins J W, Rosenlof K H, Laube J C, Röckmann T, Marsh D R and Andrews A E 2017 Quantification of the SF_6 lifetime based on mesospheric loss measured in the stratospheric polar vortex *J. Geophys. Res.: Atmos.* **122** 4626–38
[5] Masson-Delmotte V *et al* (eds) 2021 IPCC, 2021: climate change 2021: The physical science basis. contribution of working group I to the sixth assessment report of the intergovernmental panel on climate change *Technical Report* Cambridge University Press, Cambridge, United Kingdom and New York, NY, USA (https://doi.org/10.1017/9781009157896)
[6] Kieffel Y, Irwin T, Ponchon P and Owens J 2016 Green Gas to replace SF_6 in electrical grids *IEEE Power Energy Mag.* **14** 32–39
[7] Rabie M and Franck C M 2018 Assessment of eco-friendly gases for electrical insulation to replace the most potent industrial greenhouse gas SF_6 *Environ. Sci. Technol.* **52** 369–80
[8] Nechmi H E, Beroual A, Girodet A and Vinson P 2016 Fluoronitriles/CO_2 gas mixture as promising substitute to SF_6 for insulation in high voltage applications *IEEE Trans. Dielectr. Electr. Insul.* **23** 2587–93
[9] Zhang X, Li Y, Xiao S, Tian S, Deng Z and Tang J 2017 Theoretical study of the decomposition mechanism of environmentally friendly insulating medium C_3F_7CN in the presence of H_2O in a discharge *J. Phys. D: Appl. Phys.* **50** 325201
[10] Fu Y, Yang A, Wang X and Rong M 2019 Theoretical study of the decomposition mechanism of C_4F_7N *J. Phys. D: Appl. Phys.* **52** 245203
[11] Chen Li, Zhang B, Xiong J, Li X and Murphy A B 2019 Decomposition mechanism and kinetics of iso-C4 perfluoronitrile (C_4F_7N) plasmas *J. Appl. Phys.* **126** 163303
[12] Chen Li, Zhang B, Yang T, Deng Y, Li X and Murphy A B 2020 Thermal decomposition characteristics and kinetic analysis of C_4F_7N/CO_2 gas mixture *J. Phys. D: Appl. Phys.* **53** 055502
[13] Li Y, Zhang X, Zhang J, Xie C, Shao X, Wang Z, Chen D and Xiao S 2020 Study on the thermal decomposition characteristics of C_4F_7N–CO_2 mixture as eco-friendly gas-insulating medium *High Volt.* **5** 46–52
[14] Xiao S, Shi S, Li Y, Ye F, Li Y, Tian S, Tang J and Zhang X 2021 Review of decomposition characteristics of eco-friendly gas insulating medium for high-voltage gas-insulated equipment *J. Phys. D: Appl. Phys.* **54** 373002
[15] Nechmi H E, Beroual A, Girodet A and Vinson P 2017 Effective ionization coefficients and limiting field strength of fluoronitriles-CO_2 mixtures *IEEE Trans. Dielectr. Electr. Insul.* **24** 886–92

[16] Chachereau A, Hösl A and Franck C M 2018 Electrical insulation properties of the perfluoronitrile C_4F_7N *J. Phys. D: Appl. Phys.* **51** 495201

[17] Qin Z, Long Y, Shen Z, Chen C, Guo L and Zhou W 2019 Ionization and attachment coefficients in C_4F_7N gas measured by the steady-state townsend method *Appl. Sci.* **9** 3686

[18] Yi C, Yuan Z, Tu Y, Zhang Y and Wang C 2020 Measurements of discharge parameters in C_3F_7CN/CO_2 and C_3F_7CN/N_2 gas mixtures by SST *IEEE Trans. Dielectr. Electr. Insul.* **27** 1015–21

[19] Long Y, Guo L, Chen C, Shen Z, Chen Y, Li F and Zhou W 2020 Measurement of ionization and attachment coefficients in C_4F_7N/CO_2 gas mixture as substitute gas to SF_6 *IEEE Access* **8** 76790–5

[20] Zhang B, Xiong J, Hao M, Yao Y, Li X and Murphy A B 2022 Pulsed townsend measurement of electron swarm parameters in C_4F_7N– CO_2 and C_4F_7N– N_2 mixtures as eco-friendly insulation gas *J. Appl. Phys.* **131** 033304

[21] Tu Y, Cheng Y, Wang C, Ai X, Zhou F and Chen G 2018 Insulation characteristics of fluoronitriles/CO_2 gas mixture under DC electric field *IEEE Trans. Dielectr. Electr. Insul.* **25** 1324–31

[22] Zhang B, Uzelac N and Cao Y 2018 Fluoronitrile/CO_2 mixture as an eco-friendly alternative to SF_6 for medium voltage switchgears *IEEE Trans. Dielectr. Electr. Insul.* **25** 1340–50

[23] Zhao H, Li X, Tang N, Jiang X, Guo Z and Lin H 2018 Dielectric properties of fluoronitriles/CO_2 and SF_6/N_2 mixtures as a possible SF_6-substitute gas *IEEE Trans. Dielectr. Electr. Insul.* **25** 1332–9

[24] Zhang X, Chen Q, Zhang J, Li Y, Xiao S, Zhuo R and Tang J 2019 Experimental study on power frequency breakdown characteristics of C_4F_7N/CO_2 gas mixture under quasi-homogeneous electric field *IEEE Access* **7** 19100–8

[25] Nechmi H E, Slama M E A, Haddad A and Wilson G 2020 AC volume breakdown and surface flashover of a 4% Novec^{TM} 4710/96% CO_2 gas mixture compared to CO_2 in highly nonhomogeneous fields *Energies* **13** 1710

[26] Zhang T, Zhou W, Yu J and Yu Z 2020 Insulation properties of C_4F_7N/CO_2 mixtures under lightning impulse *IEEE Trans. Dielectr. Electr. Insul.* **27** 181–8

[27] Zhou W, Zhang T and Wang L 2020 Breakdown characteristics of C_4F_7N/CO_2 mixtures under steep-wavefront impulse voltages *IEEE Access* **8** 29291–8

[28] Eddine Nechmi H, Michelarakis M, Haddad A and Wilson G 2021 Clarifications on the behavior of alternative gases to SF_6 in divergent electric field distributions under AC voltage *Energies* **14** 1065

[29] Bahdad F O, Chen L, Ranjan P and Rowland S 2022 Effects of DC polarity and field uniformity on breakdown of SF_6 and C_3F_7CN/CO_2 mixture *IEEE Trans. Dielectr. Electr. Insul.* **29** 2227–35

[30] Lin X, Zhang J, Xu J, Zhong J, Song Y and Zhang Y 2022 Dynamic dielectric strength of C_3F_7CN/CO_2 and C_3F_7CN/N_2 gas mixtures in high voltage circuit breakers *IEEE Trans. Power Deliv.* **37** 4032–41

[31] Zheng Y, Yan X, Chen W, Zhou W, Shizhuo S and Li H 2019 Calculation of electrical insulation of C_4F_7N/CO_2 mixed gas by avalanche characteristics of pure gas *Plasma Res. Express* **1** 025013

[32] Zhang B, Chen Li, Li X, Guo Z, Pu Y and Tang N 2020 Evaluating the dielectric strength of promising SF_6 alternatives by DFT calculations and DC breakdown tests *IEEE Trans. Dielectr. Electr. Insul.* **27** 1187–94

[33] Zheng Y, Zhou W, Li H and Ma C 2020 Experimental and calculation study on insulation strength of C_4F_7N/CO_2 at low temperature *IEEE Trans. Dielectr. Electr. Insul.* **27** 1102–9

[34] Nijdam S, Teunissen J and Ebert U 2020 The physics of streamer discharge phenomena *Plasma Sources Sci. Technol.* **29** 103001

[35] Vu-Cong T, Toigo C, Ortiz G, Dalstein M, Jacquier F and Girodet A 2020 Numerical simulation of partial discharge current pulse: comparison between SF_6, Fluoronitrile– CO_2 mixture and Fluoroketone– CO_2 mixture *2020 IEEE Conf. on Electrical Insulation and Dielectric Phenomena* (*CEIDP*) pp 403–6

[36] Wang F, Wang L, Chen S, Sun Q, Zhong L and Zhuang C 2021 Numerical simulation of the discharge dynamics of C_4F_7N-N_2 and the influence of buffer gas *IEEE Trans. Plasma Sci.* **49** 2048–54

[37] Fan B, Zhou X, Qian Y and Zang Y 2022 Simulation of positive surface discharge in C_4F_7N gas mixture *2022 7th Asia Conf. on Power and Electrical Engineering* (*ACPEE*) pp 1604–8

[38] Gao Q, Wang X, Adamiak K, Qi X, Yang A, Liu D, Niu C and Zhang J 2022 Negative corona discharge mechanism in C_4F_7N-CO_2 and C_4F_7N-N_2 mixtures *AIP Adv.* **12** 095101

[39] Yan X, Zhou X, Li Z, Qian Y and Sheng G 2023 Numerical simulation of streamer discharge with different electrode shapes in C_4F_7N *AIP Adv.* **13** 035238

[40] Yan X, Zhou X, Li Z, Qian Y and Sheng G 2023 Surface discharge characteristics and numerical simulation in C_4F_7N/CO_2 mixture *Appl. Sci.* **13** 1409

[41] Petrović Z Lj, Dujko S, Marić D, Malović G, Nikitović Ž, Šašić O, Jovanović J, Stojanović V and Radmilović-Radenović M 2009 Measurement and interpretation of swarm parameters and their application in plasma modelling *J. Phys. D: Appl. Phys.* **42** 194002

[42] Zhang B, Xiong J, Chen Li, Li X and Murphy A B 2020 Fundamental physicochemical properties of SF_6-alternative gases: a review of recent progress *J. Phys. D: Appl. Phys.* **53** 173001

[43] Xiong J, Li X, Wu J, Guo X and Zhao H 2017 Calculations of total electron-impact ionization cross sections for fluoroketone $C_5F_{10}O$ and Fluoronitrile C_4F_7N using modified Deutsch–Märk formula *J. Phys. D: Appl. Phys.* **50** 445206

[44] Wang F, Dun Q, Chen S, Zhong L, Fan X and Li Li 2019 Calculations of total electron impact ionization cross sections for fluoroketone and fluoronitrile *IEEE Trans. Dielectr. Electr. Insul.* **26** 1693–700

[45] Zhong L, Xu J, Wang X and Rong M 2019 Electron-impact ionization cross sections of new SF_6 replacements: A method of combining Binary-Encounter-Bethe (BEB) and Deutsch-Märk (DM) formalism *J. Appl. Phys.* **126** 193302

[46] Ranković M, Chalabala J, Zawadzki M, Kočišek J, Slavíček P and Fedor J 2019 Dissociative ionization dynamics of dielectric gas C_3F_7CN *Phys. Chem. Chem. Phys.* **21** 16451–8

[47] Ranković M, Ragesh Kumar T P, Nag P, Kočišek J and Fedor J 2020 Temporary anions of the dielectric gas C_3F_7CN and their decay channels *J. Chem. Phys.* **152** 244304

[48] Sinha N, Manishkumar Patel V and Antony B 2020 Ionization cross sections for plasma relevant molecules *J. Phys. B: At. Mol. Opt. Phys.* **53** 145101

[49] Zhang J, Sinha N, Jiang M, Wang H, Li Y, Antony B and Liu C 2022 DC breakdown characteristics of C_4F_7N/CO_2 mixtures with particle-in-cell simulation *IEEE Trans. Dielectr. Electr. Insul.* **29** 1005–10

[50] Zhang B, Hao M, Yao Y, Xiong J, Li X, Murphy A B, Sinha N, Antony B and Ambalampitiya H B 2023 Determination and assessment of a complete and self-consistent electron-neutral collision cross-section set for the C_4F_7N molecule *J. Phys. D: Appl. Phys.* **56** 134001

[51] Hösl A, Chachereau A, Pachin J and Franck C M 2019 Identification of the discharge kinetics in the

perfluoro-nitrile C_4F_7N with swarm and breakdown experiments *J. Phys. D: Appl. Phys.* **52** 235201
[52] Teunissen J and Ebert U 2016 3D PIC-MCC simulations of discharge inception around a sharp anode in nitrogen/oxygen mixtures *Plasma Sources Sci. Technol.* **25** 044005
[53] Wang Z, Sun A and Teunissen J 2022 A comparison of particle and fluid models for positive streamer discharges in air *Plasma Sources Sci. Technol.* **31** 015012
[54] Verlet L 1967 Computer 'Experiments' on classical fluids. I. Thermodynamical properties of lennard-jones molecules *Phys. Rev.* **159** 98–103
[55] Koura K 1986 Null-collision technique in the direct-simulation Monte Carlo method *Phys. Fluids* **29** 3509
[56] Teunissen J and Ebert U 2014 Controlling the weights of simulation particles: adaptive particle management using k-d trees *J. Comput. Phys.* **259** 318–30
[57] Teunissen J and Ebert U 2018 Afivo: a framework for quadtree/octree AMR with shared-memory parallelization and geometric multigrid methods *Comput. Phys. Commun.* **233** 156–66
[58] Teunissen J and Schiavello F 2023 Geometric multigrid method for solving Poisson's equation on octree grids with irregular boundaries *Comput. Phys. Commun.* **286** 108665
[59] XJTUAETLab database (C_4F_7N) (available at: www.lxcat.net) (Accessed 26 April 2023)
[60] IST-Lisbon database (CO_2) (available at: www.lxcat.net) (Accessed 26 April 2023)
[61] Grofulović M, Alves L L and Guerra V 2016 Electron-neutral scattering cross sections for CO_2: a complete and consistent set and an assessment of dissociation *J. Phys. D: Appl. Phys.* **49** 395207
[62] Phelps database (N_2, O_2) (available at: www.lxcat.net) (Accessed 26 April 2023)
[63] Hagelaar G J M and Pitchford L C 2005 Solving the Boltzmann equation to obtain electron transport coefficients and rate coefficients for fluid models *Plasma Sources Sci. Technol.* **14** 722–33
[64] Seeger M, Avaheden J, Pancheshnyi S and Votteler T 2017 Streamer parameters and breakdown in CO_2 *J. Phys. D: Appl. Phys.* **50** 015207
[65] Seeger M, Votteler T, Ekeberg J, Pancheshnyi S and Sánchez L 2018 Streamer and leader breakdown in air at atmospheric pressure in strongly non-uniform fields in gaps less than one metre *IEEE Trans. Dielectr. Electr. Insul.* **25** 2147–56
[66] Pancheshnyi S 2014 Photoionization produced by low-current discharges in O_2, air, N_2 and CO_2 *Plasma Sources Sci. Technol.* **24** 015023
[67] Nijdam S, Wormeester G, van Veldhuizen E M and Ebert U 2011 Probing background ionization: Positive streamers with varying pulse repetition rate and with a radioactive admixture *J. Phys. D: Appl. Phys.* **44** 455201
[68] Childs H *et al* 2012 VisIt: an end-user tool for visualizing and analyzing very large data *High Performance Visualization–Enabling Extreme-Scale Scientific Insight* (Chapman and Hall/CRC) pp 357–72
[69] Guo B, Li X, Ebert U and Teunissen J 2022 A computational study of accelerating, steady and fading negative streamers in ambient air *Plasma Sources Sci. Technol.* **31** 095011
[70] Bujotzek M, Seeger M, Schmidt F, Koch M and Franck C 2015 Experimental investigation of streamer radius and length in SF_6 *J. Phys. D: Appl. Phys.* **48** 245201
[71] Francisco H, Bagheri B and Ebert U 2021 Electrically isolated propagating streamer heads formed by strong electron attachment *Plasma Sources Sci. Technol.* **30** 025006
[72] Allen N L and Boutlendj M 1991 Study of the electric fields required for streamer propagation in humid air *IEE Proc.* A **138** 37
[73] Li X, Guo B, Sun A, Ebert U and Teunissen J 2022 A computational study of steady and stagnating positive streamers in N_2– O_2 mixtures *Plasma Sources Sci. Technol.* **31** 065011
[74] Li X, Sun A and Teunissen J 2023 The effect of photoionization on positive streamers in CO_2 studied with 2D particle-in-cell simulations (arXiv:2304.01531)
[75] Nijdam S, van de Wetering F M J H, Blanc R, van Veldhuizen E M and Ebert U 2010 Probing photo-ionization: experiments on positive streamers in pure gases and mixtures *J. Phys. D: Appl. Phys.* **43** 145204
[76] Teunissen J and Ebert U 2017 Simulating streamer discharges in 3D with the parallel adaptive Afivo framework *J. Phys. D: Appl. Phys.* **50** 474001
[77] Long Y, Guo L, Shen Z, Chen C, Chen Y, Li F and Zhou W 2019 Ionization and attachment coefficients in C_4F_7N/N_2 gas mixtures for use as a replacement to SF_6 *IEEE Trans. Dielectr. Electr. Insul.* **26** 1358–62
[78] Briels T M P, Kos J, Winands G J J, van Veldhuizen E M and Ebert U 2008 Positive and negative streamers in ambient air: measuring diameter, velocity and dissipated energy *J. Phys. D: Appl. Phys.* **41** 234004
[79] Starikovskiy A Yu and Aleksandrov N L 2020 How pulse polarity and photoionization control streamer discharge development in long air gaps *Plasma Sources Sci. Technol.* **29** 075004
[80] Babaeva N Y, Tereshonok D V and Naidis G V 2016 Fluid and hybrid modeling of nanosecond surface discharges: effect of polarity and secondary electrons emission *Plasma Sources Sci. Technol.* **25** 044008
[81] Abbas M F, He Y L, Sun G Y, Sun A B, Eldin E T and Ghoneim S S M 2023 Positive streamer initiation in SF_6/CO_2 based on Zener's field ionization *IEEE Access* **11** 91767–76